Biofabrication

International Society for Biofabrication

ACCEPTED MANUSCRIPT

Dynamic photopolymerization produces complex microstructures on hydrogels in a moldless approach to generate a 3D intestinal tissue model

To cite this article before publication: Albert G Castaño *et al* 2019 *Biofabrication* in press https://doi.org/10.1088/1758-5090/ab0478

IOP Publishing Journal Title
Journal **XX** (XXXX) XXXXXX https://doi.org/XXXX/XXXX

Dynamic Photopolymerization Produces Complex Microstructures on Hydrogels in a Moldless approach to Generate a 3D Intestinal Tissue Model

Albert G. Castaño[1], María García-Díaz[1], Núria Torras[1], Gizem Altay[1], Jordi Comelles[1] and Elena Martínez[1,2,3]

[1] Institute for Bioengineering of Catalonia (IBEC), The Barcelona Institute of Science and Technology (BIST), Barcelona, Spain
[2] Centro de Investigación Biomédica en Red (CIBER), Madrid, Spain
[3] Department of Electronics and Biomedical Engineering, University of Barcelona, Barcelona, Spain

E-mail: emartinez@ibecbarcelona.eu

Received xxxxxx
Accepted for publication xxxxxx
Published xxxxxx

Abstract

Epithelial tissues contain three-dimensional (3D) complex microtopographies that are essential for proper performance. These microstructures provide cells with the physicochemical cues needed to guide their self-organization into functional tissue structures. However, most *in vitro* models do not implement these 3D architectural features. The main problem is the availability of simple fabrication techniques that can reproduce the complex geometries found in native tissues on the soft polymeric materials required as cell culture substrates. In this study reaction-diffusion mediated photolithography is used to fabricate 3D microstructures with complex geometries on poly(ethylene glycol)-based hydrogels in a single step and moldless approach. By controlling fabrication parameters such as the oxygen diffusion/depletion timescales, the distance to the light source and the exposure dose, the dimensions and geometry of the microstructures can be well-defined. In addition, copolymerization of poly(ethylene glycol) with acrylic acid improves control of the dynamic reaction-diffusion processes that govern the free-radical polymerization of highly-diluted polymeric solutions. Moreover, acrylic acid allows adjusting the density of cell adhesive ligands while preserving the mechanical properties of the hydrogels. The method proposed is a simple, single-step, and cost-effective strategy for producing models of intestinal epithelium that can be easily integrated into standard cell culture platforms.

Keywords: microengineered 3D tissue models, poly(ethylene glycol) hydrogels, photopolymerization, 3D microstructures, intestinal epithelium

1. Introduction

Three-dimensional (3D) microstructures such as compact folds, invaginations, evaginations, and wavy morphologies are common in invertebrate and vertebrate animals, particularly in epithelial tissues. These microstructures are formed during tissue development and are key to their proper functioning. In the small intestine, crypts and villi provide the tissue with a large surface area. This increases the volume and residence time of the fluids trapped between villi, improving its absorbance function. In addition, 3D microstructures provide an oxygen depleted microenvironment for the microbiota and compartmentalize the multiple cell types composing the

tissue. Villi are finger-like protrusions, 0.2-1 mm in height, 100-200 μm in diameter, and have a density of 20-40 villi mm^{-2} [1–3]. Despite its physiological relevance, this 3D complex architecture is omitted in standard *in vitro* models of the small intestine. Conventional models are based on flat monolayers of cell lines such as Caco-2 cells, grown on filter supports that provide separate access to the luminal and basolateral side of the monolayer. These conventional two-dimensional (2D) models have been essential as screening tools for drug development, but recent publications demonstrate that the predictive capacity of current preclinical assays is not optimal [4]. Improved *in vitro* models rely on providing cells with a more physiologically realistic environment, including tissue architecture, cell-matrix interactions and biomimetic chemical and mechanical signaling [4–8]. Hydrogels have been proposed as alternative cell culture substrates. They are hydrophilic polymers with high water content and they provide a friendly environment for cell growth and differentiation. They also have a broad range of mechanical properties compatible with soft tissue microenvironments (< 40 kPa) [9]. This level of softness, however, hampers 3D hydrogel shaping to simulate the topographies found at the tissue level. The main limitation is the difficulty in microfabricating soft materials with complex 3D geometries, high aspect ratio and curvature using efficient and simple methods which could be routinely implemented in standard assays. Microfabrication techniques such as conventional replica molding and direct printing are typically restricted to the fabrication of low to medium aspect ratio microstructures with perpendicular walls [10]. Several variations of replica molding techniques including the use of laser ablation and sacrificial molds can produce soft 3D microstructures [10,11]. These procedures use complex equipment and multiple fabrication steps to overcome the difficulties in demolding the soft microstructures. Photopolymerization-based microfabrication techniques such as photolithography, soft lithography or stereolithography are well established to produce microstructures without the need for molding and demolding steps. While stereolithography requires sophisticated optical set ups and it is based on layer-by-layer photopolymerization [12], conventional photolithography is a much more simpler technique that has been widely used for micropatterning in various fields. Typically, it is based on the crosslinking of a photoresist through a 2D photomask with a desired pattern upon exposure to collimated UV light. Photolithography has been traditionally used to produce microstructures with simple geometries on hydrogels of synthetic polymers such as poly(2-hydroxyethyl methacrylate) and polyethylene glycol (PEG) derivatives [13–15]. Shim *et al.* demonstrated the suitability of the photolithography technique for producing 3D microstructures with complex morphologies on hard photocurable resins that undergo free radical polymerization [16,17]. This was done by establishing controlled oxygen gradients within the polymerization set up. The Damköhler number, Da, (ratio of characteristic oxygen diffusion to oxygen depletion times) controls the polymerization reaction. When Da ~ 1, which can be achieved by including a source of oxygen in the polymerization system, objects with conical shapes can be formed [16,17].

In this study, we propose to exploit the potential benefits of reaction-diffusion mediated photolithography in the production of 3D cell culture substrates for biomedical applications. For this purpose, we demonstrate that by the proper tuning of the polymer composition and the fabrication parameters we can faithfully mimic the 3D architecture of the small intestinal epithelium in synthetic hydrogels. We used a system design in which the Damköhler number significantly changes with the distance to the polymerization light source. Through this strategy, we demonstrate that villi-like microstructures of anatomic and predictable dimensions can be easily fabricated using poly(ethylene glycol) diacrylate (PEGDA) polymer. The reaction-diffusion process is not straightforward when applied to create complex 3D structures on hydrogels from solutions with low polymer concentrations. In diluted solutions, the free radical polymerization proceeds longer, and the diffusion of the radicals into unexposed regions leads to incomplete crosslinking at the boundaries between polymerized and unpolymerized material [18]. The crosslinking density affects the mechanical properties of the material, and therefore the cellular adhesion and response [19]. To gain control on cell-surface interactions, it is crucial to accurately control the properties at the boundaries. Copolymerization is an attractive technique as a route to functionalize polymers with tunable properties. The copolymerization of PEGDA with acrylic acid (AA) has been shown to tune hydrogel properties such as crosslinking density and swelling behavior [20,21]. In the presence of oxygen, AA affects the termination rate of the free radical polymerization [22], leading to a confinement of the crosslinking volume and therefore minimizing the tacky surfaces resulting from incomplete poplymerization. Moreover, the copolymerization of PEGDA with AA provides the material with carboxylic groups that allow the controlled immobilization of cell adhesive ligands. Synthetic polymers such as PEGDA have advantages over natural polymers. These include adjustable mechanical properties and non-biodegradability to withstand long term cell culture conditions [23]. However, PEGDA-based hydrogels are intrinsically nonadhesive for cells and their bioactive modification is essential for cell culture applications. Bioactive hydrogels are usually obtained by copolymerization with extracellular matrix (ECM)-based peptides or proteins that have been previously chemically modified with reactive groups such as acrylates [24,25]. In our approach, the copolymerization of PEGDA-AA allows the covalently immobilization of unmodified ECM proteins and

renders the material suitable for cell culture (Figure 1(a)). By adjusting the amount of AA, the ligand density on the material can be fine-tuned while preserving the mechanical properties of the hydrogels.

The 3D villi-like scaffolds were successfuly fabricated onto porous filter membranes allowing the monitoring standard functional properties of the intestinal cell barrier such as its integrity and permeability. Caco-2 cells seeded on the 3D scaffolds formed monolayers of differentiated enterocytes with transepithelial electrical resistance (TEER) values that were significantly closer to *in vivo* values than conventional cell monolayers. These results demonstrate that this moldless microfabrication technology is an easy-to-use tool that can faithfully replicate 3D microtopographies at the tissue level in hydrogels. It can provide cells with a more realistic microenvironment, including cell-to-matrix interactions and proper chemical and mechanical signaling, while remaining compatible with standard cell characterization techniques.

2. Materials and methods

2.1 Materials

Poly(ethylene glycol) diacrylate (PEGDA) (Mn 6000 g mol^{-1}), 2-Hydroxy-4′-(2-hydroxyethoxy)-2-methylpropiophenone (Irgacure D-2959) photoinitiator, (1-ethyl-3-(3-dimethylaminopropyl)carbodiimide hydrochloride) (EDC), N-Hydroxysuccinimide (NHS), Acrylic acid (AA) and Hank's Balanced Salt Solution (HBSS) were purchased from Sigma-Aldrich. Phosphate buffered saline (PBS) and BupH MES buffered saline were from ThermoFisher. Polydimethylsiloxane (PDMS) Sylgard 184 was from Dow Corning. Collagen type I, fibronectin and laminin were from Sigma-Aldrich. Fluorescein-isothiocyanate (FITC) dextran of 4 kDa (FD4) was from Sigma-Aldrich. Streptavidin Texas Red® was from ThermoFisher. Fluoromont-G mounting solution was from SouthernBiotech.

2.2 Fabrication of PEGDA-AA villi-like scaffolds

A chip fabricated with 1 mm thick PDMS stencil containing an array of pools on a black coated polystyrene support was used for hydrogel UV polymerization (Figure S1). Briefly, PDMS prepolymer was prepared at a ratio 10:1 w/w with the curing agent. The prepolymer solution was casted between two flat poly(methyl methacrylate) sheets spaced 1 mm apart and cured for 24 h at room temperature. Pools, either 6.5 or 10 mm in diameter, were punched, and two inlets and channels connecting them were carved, with a 1.5 mm punch and a scalpel, respectively, to introduce the hydrogel solution (Figure 1(b)). Silanized glass coverslips of 12 mm in diameter or Tracketch® polyethylene terephthalate (PET) membranes of 5 µm pore size (Sabeu GmbH & Co) were then used to cover the tops of the PDMS pools. Prepolymer solutions containing 6.5% w/v PEGDA, 0 to 1.2% w/v AA, and 1% w/v Irgacure D-2959 were dissolved in PBS at 65 ºC for 1 h, filtered and flown into the chip. Villi-like micropillars were fabricated by placing patterned photomasks on top of the glass coverslips or porous membranes. Photomasks had pattern designs consisting of arrays of circular UV-transparent windows 50 µm in radius at a density of 25 windows mm^{-2}. These were designed using AutoCAD software (Autodesk) and printed on acetate films (CAD/Art Services Inc.). Pattern dimensions were selected to match the structures found in small intestinal tissue [1,3]. UV light exposure was performed in a MJBA mask aligner (SUSS MicroTech), using a power density of 25 mW cm^{-2} measured at 365 nm wavelength (SUSS MicroTech). Prepolymer solutions were exposed for 60 to 220 s to form the micropillars. After UV exposure, unreacted polymer and photoinitiator were washed out with PBS. When required, hydrogel disc samples were also fabricated by light flood exposure, without photomask. Samples were kept submerged in PBS at 4 ºC for at least three days to reach equilibrium swelling. During the swelling period, PBS was exchanged every day to remove uncrosslinked polymer molecules. After swelling, cross-sections of microstructured hydrogels were obtained using a scalpel. Sample cross-sections were imaged by bright field microscopy using a Nikon Eclipse Ts2 instrument to determine their morphology and dimensions (Figure S2). The morphology of the microstructured scaffolds was also assessed by scanning electron microscopy (SEM). Samples were sequentially dehydrated in ethanol followed by critical point drying (K850, Quorum technologies). Samples were then imaged by SEM (NovaTM NanoSEM 230, FEI).

2.3 Assembly of PEGDA-AA hydrogels on modified Transwell® inserts

PEGDA-AA hydrogel scaffolds, fabricated on porous PET membranes, were mounted on standard 24-well polycarbonate Transwell® filter inserts (Corning Costar) using double-sided pressure-sensitive adhesive (PSA) rings (Adhesives Research) (Figure S3). The inserts form two compartments (apical and basolateral) that mimic the luminal and stromal parts of the intestinal tissue barrier. Briefly, the standard polycarbonate (PC) membrane from the Transwell® inserts was carefully removed with a scalpel and replaced by the PET membrane containing the hydrogel on top and then fixed by the double-sided PSA ring. Immediately after, pressure was applied for 15 min at RT to assure proper sealing. Then, a drop of sterile PBS buffer supplemented with 10% v/v penicillin/streptomycin and 1:500 Normocin (InvivoGen) was added on top of the hydrogels to prevent them from drying. Later, extra 200 µL and 600 µL of the same PBS buffer solution were added to the apical and basolateral Transwell® cavities, respectively, and the inserts were stored at 4 ºC until further use. All the assembly process was performed under sterile conditions.

2.4 Characterization of PEGDA-AA hydrogels

The copolymerization of PEGDA-AA was characterized by Fourier-transform infrared spectroscopy (FTIR) in a Nicolet iS 10 instrument (ThermoFisher Scientific), using an ATR diamond and a DTGS detector. Hydrogel discs (12 mm diameter, 2 mm height.) were prepared from prepolymer solutions of 10% w/v PEGDA and AA concentrations ranging 0 to 1.2% w/v. Hydrogels were polymerized for 300 s to ensure full crosslinking. All samples were rinsed with Milli-Q water and allowed to dry for 24 h in a vacuum desiccator before being analyzed by FTIR. Scans in the range of 500-4000 cm^{-1} were performed with a resolution of 4 cm^{-1}. Spectra reported correspond to the average of 16 scans. To determine the effects of acrylic acid on the bulk mechanical properties of the samples, hydrogel discs (10 mm diameter, 2 mm height) were obtained by polymerizing solutions of 6.5% w/v and AA concentrations ranging from 0 to 1.2% w/v for 150 s. Hydrogels were allowed to reach equilibrium swelling for 3 days in PBS. After swelling, sample diameters differed among them, so swollen hydrogels were punched to obtain 10 mm diameter samples. Stress-strain curves in compression were recorded with a Zwicki Z0.5TN machine (Zwick-Roell). To avoid drying of hydrogels, a few drops of PBS were added just before the beginning of each measurement. Stress-strain curves were obtained with a speed of 2 mm min^{-1}, limiting the strain rate to 1% min^{-1} and the maximum strain to 10% [26]. An initial load of 5 mN was applied to promote the adequate contact between the hydrogel and the compression plates. The Young's modulus of the bulk hydrogels was calculated as the slope of the linear part of the stress-strain curves. Since the height of each hydrogel was also recorded from the mechanical testing, this was used to determine the swelling ratio [24]. The height of each hydrogel after swelling was compared with its height immediately after fabrication.

To investigate potential differences on the mechanical properties of the bulk and the surface of the hydrogel scaffolds due to the fabrication process, Atomic Force Microscopy (AFM) was employed. AFM indentations were performed on the surface of microstructured scaffolds fabricated using solutions containing 6.5% w/v PEGDA, 0.3% w/v AA. Samples were produced on glass coverslips and exposed 120 s with the photomask followed by a flood exposure of 120 s. Measurements were done using a JPK Nanowizard 4 machine (JPK Instruments) with a V-shaped cantilever with a quadratic pyramidal tip of 35° (Θ) face angle, and a nominal spring constant (k) of 0.08 N/m (PNP-TR-20, Nanoworld). After calibration of the sensitivity, series of local force-displacement (F-z) curves were measured at several points on the surface of the villi-like hydrogel scaffolds, including tip and base regions. Samples were indented up to 5 µm from the surface. The values of the local surface stiffness were obtained by applying Hook's law and the Hertz model for a quadratic pyramidal tip to the force-displacement curves.

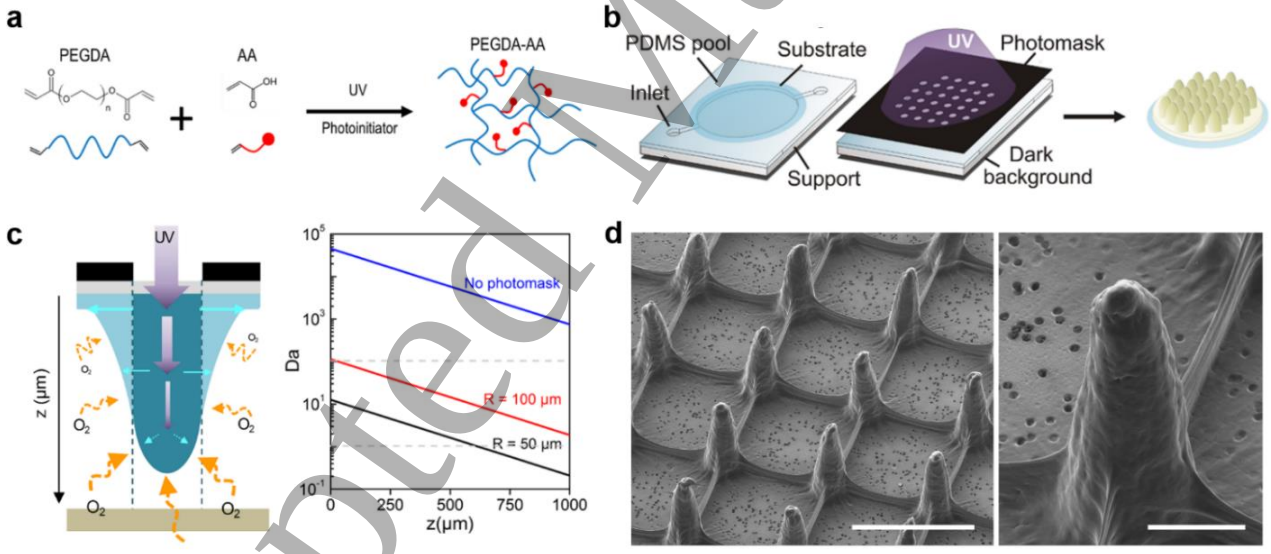

Figure 1. Dynamic photopolymerization approach for single-step, moldless microfabrication of villi-like hydrogel scaffolds. **(a)** Scheme for copolymerization of PEGDA and acrylic acid (AA) in the presence of the photoinitiator with UV radiation. **(b)** Schematic illustration of the single-step photolithography process. The substrate can be a cover glass or a porous membrane **(c)** Oxygen effects create dynamic polymerization conditions on the fabrication process. Left: Schematic illustration of the convolution of the attenuation of light (violet arrows) and the diffusion of oxygen along the vertical axis *z*. Dashed line indicates the boundary of the photomask window. Right: Plot of Damköhler number as a function of the vertical axis *z* varying the photomask window radii. **(d)** SEM images of hydrogel microstructures fabricated on a porous membrane (pores are seen at the base due to sample preparation process). Left: Scale bar = 200 µm. Right: Scale bar = 100 µm.

2.5 Functionalization of PEGDA-AA villi-like scaffolds with cell adhesive proteins

After swelling, PEGDA-AA hydrogels were functionalized with laminin or collagen type I via a EDC/NHS mediated coupling. Specifically, the carboxylic groups of PEGDA-AA hydrogels were activated with a solution containing 25 mM EDC and 50 mM NHS in MES buffer (0.1 M, pH 4.7) for 30 min at room temperature. Hydrogels were then washed with PBS and further reacted with 0.01% w/v collagen type I or 50 μg mL^{-1} laminin solution overnight at 4ºC. The hydrogel activation and further protein functionalization were characterized by FTIR as previously described.

To determine the effects of AA concentration on the ligand density of the hydrogels, discs (10 mm diameter, 1 mm height) were prepared from solutions of 6.5% w/v PEGDA and AA concentrations ranging from 0 to 0.6% w/v upon 150 s of UV irradiation. Samples were activated with EDC/NHS as described above and functionalized with Streptavidin Texas Red® (0.05 mg mL^{-1}). Hydrogels were mounted with Fluoromont-G and imaged with a Leica TCS SPE confocal microscope. Discs prepared with a AA concentration of 0.9% w/v were used to test the stability of the protein functionalization to rinsing and storage time. Samples were rinsed one to 10 times and their fluorescence was evaluated by fluorescence microscopy. Analogously, samples were stored at 4 ºC in PBS for 1 to 7 days, exchanging PBS solution every day, and their fluorescence was monitored over the storage time.

2.6 Cell culture

Caco-2 cells (ATCC® HTB-37™) from passages 74 to 80 were expanded and maintained in 75 cm^2 flasks in high glucose DMEM (Gibco, Thermofisher), supplemented with 10% v/v fetal bovine serum (FBS) (Gibco, Thermofisher), 1% v/v penicillin/streptomycin (Sigma-Aldrich) and 1% v/v of non-essential amino acids (Gibco, Thermofisher). Cells were maintained in an incubator at 37ºC and 5% CO_2, changing medium every two days and passaged weekly. Cells were seeded either on the hydrogels fabricated on coverslips at a density of $5x10^5$ cells cm^{-2}, or on the hydrogels mounted on the modified insert at a density of $1.5x10^5$ or $2.5x10^5$ cells cm^{-2} for 2D discs or 3D microstructures, respectively. The surface area of the villi-like hydrogels was estimated using the formula for the area of a truncated cone without base (see Supporting Information). Control experiments were performed on cells cultured in standard 24-well polycarbonate Transwell® filter inserts (0.33 cm^2 growth area, 0.4 μm pore size) at a density of $1.5x10^5$ cells cm^{-2}. Cells were cultured for 21 days, exchanging media every other day.

2.7 Barrier integrity assessment

The intestinal epithelium forms a hihgly selective tissue barrier. The tissue barrier integrity formed by the Caco-2 cells cultured on the villi-like hydrogel scaffolds was monitored during cell culture using an standard approach. Hydrogel samples fabricated on porous membranes were mounted on Transwell® inserts and Caco-2 cells were cultured on them. The transepithelial resistance (TEER) between the two compartments formed by the inserts was measured every other day with a EVOM2 Epithelial voltohmmeter with STX3 electrode (World Precision Instruments). Measured resistance values were corrected by substracting the resistance of the membrane and the hydrogel. TEER values were normalized by the total surface area of the cell monolayer, which significanlty differ from 2D and 3D cell culture systems. After 21 days, drug permeability studies using FITC-dextran of 4.4 kDa (FD4) as a tracer were performed to monitor the paracellular transport through the tight junctions. Briefly, cells were carefully washed with HBSS buffer prior to adding 200 μL of test compound at a concentration of 0.5 mg mL^{-1} to the apical and 600 μL of HBSS buffer to the basolateral compartments. Throughout the experiment, cells were incubated at 37 ºC on a horizontal shaker at 50 rpm. Samples were withdrawn from the basolateral compartment at specific time points during 3 h followed by buffer replacement. Retrieved samples were then transferred to a 96-well black plate and their fluorescence was read on the Infinite M200 PRO Multimode microplate reader (Tecan) at 495 nm excitation and 520 nm emission wavelengths. The apparent permeability coefficient (P_{app}) was calculated by the following equation,

$$P_{app} = \frac{dQ}{dt} \cdot \frac{1}{A \cdot C_0}$$

where dQ/dt is the flux, A the area of the filter insert, and C_o the initial donor concentration of the test compound. The steady state flux was used for calculation of the P_{app} value. All experiments were done in triplicate. As a control, the flux through the hydrogels without cells was also measured to assure that the hydrogel was not limiting the permeability of the tracer.

2.8 Cell polarization assessment

Cells on the intestinal epithelium are characterized by their columnar shape and polarization, with the apical and basolateral compartments separated by tight junctions. Cell polarization was studied through the immunostaining of nuclei, filamentous actin (F-actin), and epithelial cell markers (ZO-1, β-catenin, and villin). After 21 days of culture, cells were fixed with 10% neutral buffered formalin solution (Sigma-Aldrich) at RT for 30 min, permeabilized with 0.5% Triton-X and blocked with 1% bovine serum albumin (BSA) and 3% donkey serum. Primary antibodies were used against

ZO-1 (ab190085, Abcam, UK) (2 μg mL^{-1}), β-catenin (ab2365, Abcam) (5 μg mL^{-1}) and villin (ab201989, Abcam) (1 μg mL^{-1}). The incubation was performed for 2 h at RT and overnight at 4°C. Then, samples were incubated with secondary antibodies and/or Alexa Fluor® 568 Phalloidin (ThermoFisher Scientific) for 2 h at RT. Anti-goat Alexa 568 (A11057, ThermoFisher Scientific), anti-rabbit Alexa 647 (Jackson Immunoresearch) and anti-mouse Alexa 488 (A21202, ThermoFisher Scientific) were used at 2 μg mL^{-1}. Finally, samples were incubated with a 1:5000 dilution of DAPI (ThermoFisher Scientific) for 15 min.

Cell polarization was also assessed by analyzing nuclei elongation and orientation with respect to the surface of the villi-like microstructures. Confocal microscopy images of cells cultured for 21 days on either villi-like scaffolds or conventional Transwell® inserts were used for this purpose. Results were compared with data obtained from images of histological cross sections of human small intestine [27]. Villi-like hydrogels were mounted on a 1 mm high PDMS holder to preserve microstructures morphology during image acquisition. Samples were imaged using confocal laser-scanning microscopes (TCS SPE or SP2, Leica Microsystems), acquiring z-stacks at 1 μm intervals. Images were processed by Image J software [28]. The image threshold was adjusted to individually identify cell nuclei and surface contour. Then, images were converted to binary values and nuclei were fitted to ellipses. Nuclei elongation was determined as the ratio between the major and the minor ellipse axis. Nuclei orientation with respect to the surface was computed by cell orientation index, which ranges between 1, when the major ellipse axis are normal to the surface (polarized cells), and -1, when they lay parallel to the surface (non polarized cells).

2.9 Data analysis and statistics

Graphs were plotted using OriginPro 8.5 software. In the case of normal distributions, differences between groups were compared using ANOVA. Non-parametric analyses were performed using the Mann-Whitney U and Kruskal-Wallis tests. The tests performed are specified in the respective figure legends. Differences were considered statistically significant when $p < 0.05$.

3. Results

3.1 Controlled growth of high-aspect ratio, villi-like hydrogel microstructures

Free radical polymerization can produce polymeric microstructures with complex and well-defined shapes by controlling the dynamics of the polymerization reaction and establishing oxygen gradients within the system [15–17]. Molecular oxygen inhibits radical induced polymerization because of its high reactivity with radicals, forming peroxide molecules that terminate the reaction [29]. For polymerization to take place, the concentration of oxygen needs to be locally depleted, so monomers can successfully compete with molecular oxygen for the scavenging of the initiator radicals [29]. If the system has a source of oxygen, this will diffuse towards the regions with lowered concentrations. When the timescale of oxygen diffusion is comparable to that of oxygen depletion produced by the termination reaction, the photopolymerization will stop, even if it has already been initiated [30]. Because of high surface-to-volume ratios, the inhibition of photopolymerization reactions is aggravated on the microscale [15]. To account for the relevance of oxygen diffusion within such systems, the so-called Damköhler number, Da, can be used. Da accounts for the ratio between the characteristic timescales involved in oxygen diffusion and oxygen depletion processes [16,17]. The characteristic oxygen diffusion time, τ_{diff}, depends on the oxygen diffusion coefficient within the polymer, D_0, and the size of the microstructures to be fabricated, which is defined by the radius of the transparent windows of the 2D photomask, R. The timescale of oxygen depletion, τ_{depl} can be estimated from the initial oxygen molar concentration in the solution, $[O_2]_0$, and the rate of radical formation, which depends on the photoinitiator properties φ (quantum yield of radical production) and ε (molar extinction coefficient), the photoinitiator molar concentration [PI] and the intensity of UV light I [16]. Da can be then calculated as:

$$Da = \frac{\tau_{diff}}{\tau_{depl}} = \frac{R^2/D_0}{[O_2]_0/\varphi\varepsilon[PI]I}$$

Depending on the Da value, Shim *et al.* [16] identified three growth pathways for polymeric microstructures. When Da >>1, growth does not depend on oxygen diffusion, the diameter of the microstructures is always equal to the transparent windows of the photomask, and the height of the microstructures can be controlled by the UV light irradiation time. When Da ~ 1 and the system is closed to oxygen, the microstructures will grow in laterally along the central axis of the transparent windows while maintaining height during growth (limited to the thickness of the container of the polymer solution). When Da ~ 1 and the system is open to oxygen on one of its surfaces, conical microstructures that maintain their height during growth are obtained [16,17]. In our experimental set-up (Figure 1(b)), the height of the container is significant. Due to the absorbance of light intensity by the photoinitiator, which can be estimated from the Beer-Lambert law, Da will change along the vertical axis (distance to the ligth source), *z*, as:

$$Da\,(z) = \frac{R^2/D_0}{[O_2]_0/\varphi\varepsilon[PI]I \cdot exp(-2.303\varepsilon[PI]z)}$$

For masks of R = 50 μm, a value that matches the anatomic dimensions of small intestinal villi microstructures, PEGDA hydrogels (D_0 = 1 x 10^{-10} m^2s^{-1}, $[O_2]_0$ = 1 mol m^{-3}), [15] maximum light intensity (centered at λ = 313 nm), I = 9.75·10^{-4} mol $m^{-2}s^{-1}$, and 1% w/v of Irgacure 2959 solution as photoinitiator (φ = 0.29, and ε (λ = 313 nm) = 40 m^2 mol^{-1}) [31], Da significantly changes with *z* (Figure 1(c)). Because our set-up is open to oxygen due to the PDMS pools and polystyrene support, distinguishable growing pathways were expected for different *z* values. However, while the absence of photomask rapidly produced the full polymerization of the polymer solution (Da ~ 10^4 for containers 6 mm in diameter), the presence of the photomask with 50 μm radius light windows produced finger-like micropillars of high aspect-ratio (Figure 1(d)). The height of the micropillars can be controlled by tuning a single parameter, the exposure time and micropillars up to 600 μm, corresponding to aspect ratios 1:6 (width: height) can be obtained (Figure 2). The diameter of the microstructures obtained was consistent with the dimensions of the photomask windows, and the microstructures had blunt tips like those found in the small intestinal tissue. We attribute these complex geometries to a mixture of the growth pathways defined by Shim et al [16]. Bottom-to-top growth seems to dominate for distances close to the lamp (Da ~ 10), so the microstructures grow in height while keeping their lateral dimensions to the full extent of the transparent windows of the mask. At greater distances, Da ~ 1, and conical shapes appeared. For distances above ~600 μm, polymerization was not experimentally observed in our set-up since Da < 1 and the oxygen diffusion is faster than the oxygen depletion (Figure 1c) Such a limit in the photopolymerization vertical distance can be tuned by changing the light intensity, photoinitiator concentration and photomask window size [32].

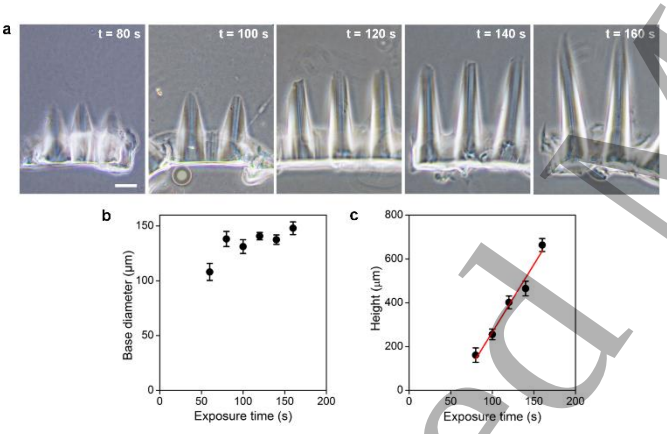

Figure 2. Effect of exposure time on microstructure base diameter, height and morphology. **(a)** Cross-sections of villi-like hydrogel scaffolds fabricated with 6.5% w/v PEGDA and 0.3% (w/v) AA and exposed for 80 to 160 s. For characterization purposes samples were produced on glass coverslips, so a flood exposure of 15 s was performed to hold them together. **(b,c)** Hydrogel total height and base diameter as a function of exposure time. Mean ± SD, n > 12. Scale bar = 100 μm

3.2 PEGDA-AA copolymers allow fine tuning of photopolymerization reaction and ligand density

Epithelial cells forming tissue barriers need to be polarized to exert their protective function. They possess an apical region facing the lumen, and a basolateral membrane facing the organ side. Cell polarity is guided by the structural features of the tissue and, in particular, by the epithelial basement membrane [33–36]. Collagen-coated membranes as well as collagen hydrogels are good supports for epithelial cell polarization [10,37]. However, it has been shown that cell-laden microstructured collagen matrices do not preserve the scaffold morphology over time due to degradation and do not allow long-term experiments [38,39]. Synthetic hydrogels based on PEG acrylates are an attractive alternative to natural hydrogels. PEGDA hydrogel networks are biocompatible and chemically versatile, allowing the incorporation of cell adhesive proteins and peptides [15].

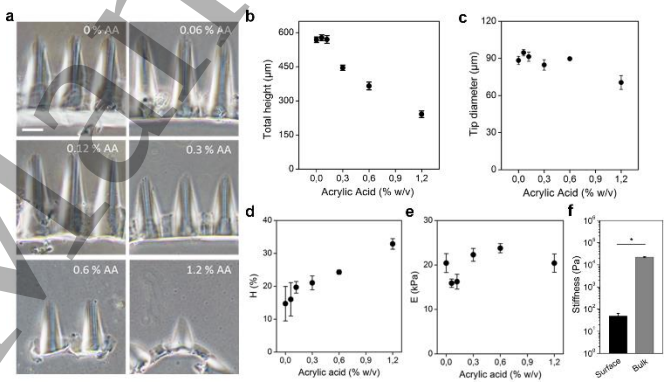

Figure 3. Effect of acrylic acid content on the polymerization reaction and the morphology of resulting microstructures. **(a)** Cross-sections of villi-like hydrogel scaffolds fabricated with 6.5% w/v PEGDA and varying concentrations of AA exposed for 120 s. For characterization purposes samples were produced on glass coverslips, so a flood exposure of 15 s was performed to hold them together. **(b,c)** Hydrogel total height and tip diameter as a function of AA concentration. **(d,e)** Hydrogel swelling ratio H and bulk Young's modulus (E) of PEGDA-AA hydrogels as a function of AA content. **(f)** Graph comparing the values of hydrogel stiffness measured at the surface (indentation depth up to 5 μm) and in bulk samples. Mean ± SD, n > 5. Scale bar = 100 μm.

When copolymerized with AA, PEGDA-AA networks have been used in cell culture applications, forming composite hydrogels with collagen [40]. In addition, PEGDA-AA copolymers have also been employed as substrates in biosensing applications [41]. We copolymerized PEGDA with

different amounts of AA ranging from 0 to 1.2% w/v. The incorporation of AA was assessed by the presence of a strong absorbance peak at 1576 cm^{-1} in the FTIR spectra, which is attributed to the asymmetric vibration of carboxyl groups, (Figure S4) [42]. Factors such as viscosity of the solution or the presence of oxygen may affect the kinetics of the reaction and the polymerization rate. The viscosity of PEGDA-AA solutions was not significantly different for solutions with increasing AA concentration (Figure S5). Therefore, we can presume that the diffusion of the species was not significantly altered. In the presence of oxygen, the termination rate for PEGDA was reported as 2.5 x 10^3 $m^3mol^{-1}s^{-1}$ [15], while the termination rate for AA polymerization was reported as 3.2 x 10^5 $m^3mol^{-1}s^{-1}$ [22]. This increase in the termination rate had an effect on the shape of the microstructures. With increasing AA concentration, significantly shorter microstructures were obtained for identical exposure times (Figure 3(a)). The total height of the pillars decreased from around 600 μm to 240 μm when AA was increased to 1.2% (w/v) (Figure 3(b)). The finger-like shape of the structures was maintained, but the tip became sharper, especially with the highest AA concentration (Figure 3(c)). Then, the production of samples with microstructure dimensions compatible with those found in the villi of small intestinal tissue are conditioned by the concentration of AA. The incorporation of AA allowed the fine tuning not only of the morphology but also of the physicochemical properties of the hydrogel [20]. The hydrogel swelling ratio increased significantly with the percentage of AA within the copolymer (Figure 3(d)). However, within the range of concentration assayed, no significant differences on the compression elastic modulus of the samples were observed (Figure 3(e)). All the bulk elastic modulus values measured for the samples were consistent with values reported for intestinal mucosa [9,43]. Trends observed in both swelling and elastic modulus values are in agreement with those previously reported for PEGDA-AA copolymers [20,44]. The increased swelling can be related to the increased amounts of carboxyl groups with increased concentrations of AA. Carboxylic groups have higher polarity than the ester groups in PEGDA, and draw more water into the crosslinked polymer network [44]. However, while bulk measurements provide a global picture of the hydrogel mechanical properties [19], cells only sense few microns into the material [45], therefore the local stiffness at the surface of the material was measured. AFM measurements demonstrated that the mechanical properties at the surface were much softer than the bulk values (Figure 3(f)). This is due to the oxygen inhibition and diffusion of radicals at the hydrogel boundaries, which has been reported to lead to incomplete crosslinking at the surface [18].

Copolymerization with AA allowed for the covalent binding of extracellular matrix proteins to the hydrogel through a carbodiimide-mediated crosslinking reaction in the presence of carboxyl groups. Samples were activated by EDC/NHS and further incubated in a protein solution (Figure 4(a)). FTIR spectra show that, after activation, the carboxylate peak of the AA, located at 1576 cm^{-1}, disappeared due to the incorporation of NHS molecules through amide bonds (Figure 4(b)). Two peaks around 1800 cm^{-1} appeared and these corresponded to the presence of NHS [46]. After incubation with collagen I, amide bands centered at 1550 and 1650 cm^{-1} were visible [47], together with a significant decrease in the absorbance of the NHS peaks. Fluorescent measurements obtained after incubation with streptavidin Texas Red® revealed that the functionalization was homogeneous along the microstructures (Figure 4(c)). The amount of immobilized protein increased with the amount of AA in the polymer solution (Figure 4(d)), which agrees with previously published data [41]. Fluorescent measurements performed after repeated washing of the sample and during a 7 days storage period revealed the covalent nature of the protein binding, as no significant differences in the fluorescence intensity levels were found after both procedures (Figure S6).

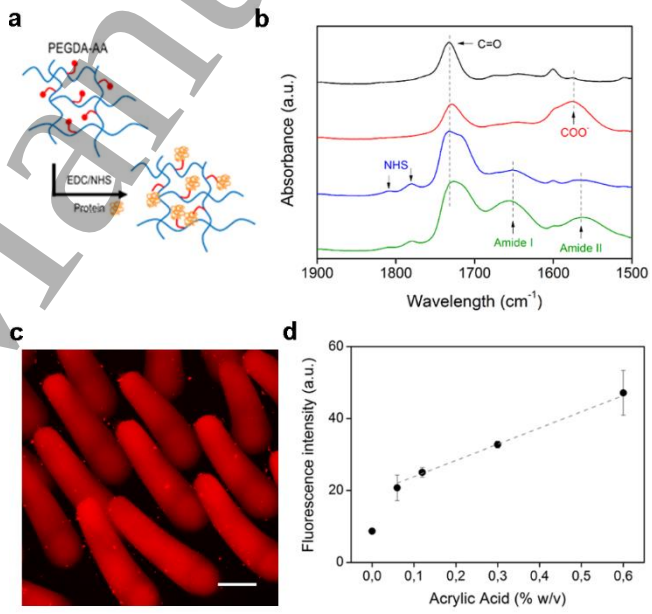

Figure 4. Functionalization of PEGDA-AA hydrogels with ECM proteins. **(a)** Scheme of the hydrogel functionalization through the EDC/NHS coupling reaction. **(b)** Detailed FTIR spectra acquired after each step of the functionalization process. PEGDA hydrogel in black, PEGDA-AA hydrogel in red, EDC/NHS activated hydrogel in blue, and collagen-functionalized hydrogel in green. **(c)** Confocal projection of microstructured PEGDA-AA hydrogel functionalized with Streptavidin-Texas Red. **(d)** Fluorescence intensity of hydrogels as a function of AA concentration after functionalization with Streptavidin-Texas Red. Mean ± SD, n = 5. Scale bar = 100 μm.

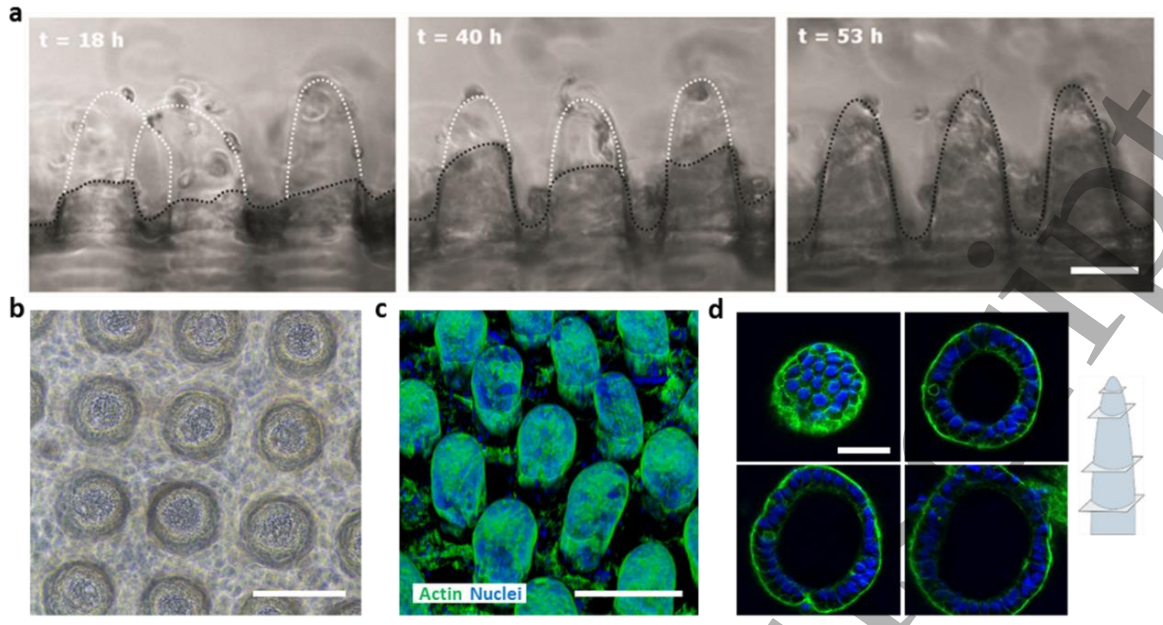

Figure 5. Caco-2 cell culture on PEGDA-AA villi-like 3D scaffolds. **(a)** Sequential frames from time-lapse microscopy of Caco-2 cells migrating upwards along the PEGDA-AA micropillars. **(b)** Top view brightfield image focused on micropillars tip and **(c)** confocal projection of Caco-2 cells grown on the 3D scaffolds for 21 d. **(d)** Detailed cross-sections of a representative Caco-2 cell covered micropillar. Nuclei are shown in blue and F-actin is shown in green. Scale bars: a = 150 μm; b and c = 200 μm; d = 50 μm.

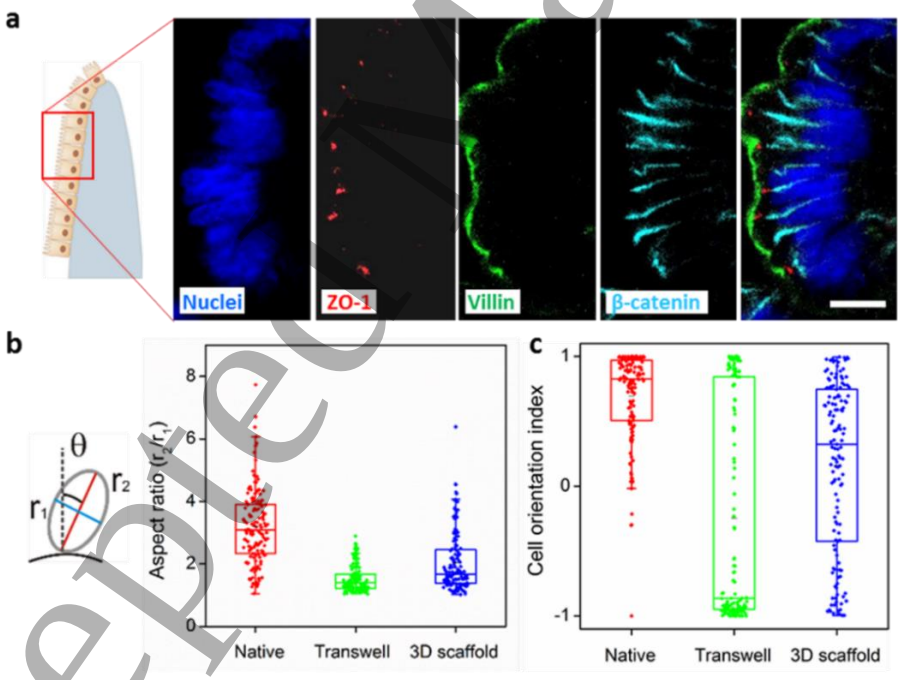

Figure 6. Caco-2 cell polarization characterization. (a) Confocal images of Caco-2 monolayer formed on the 3D scaffold showing the nuclei in blue, ZO-1 in red, villin in green and b-catenin in cyan. (b, c) Nuclei elongation and orientation analysis. The nuclei aspect ratio and cell orientation index from Caco-2 cells grown for 21 d in conventional Transwell® or in the PEGDA-AA villi-like 3D scaffolds are compared with the nuclei from a histological cross-section of a native small intestine [27]. For the boxplots, the bar shows the median, and the upper and lower boxes represent the 75% and 25% of the data, respectively. The whiskers extend to the 5% and 95%. n = 140. Scale bar = 10 μm.

Therefore, this methodology allows tuning the ligand density of the hydrogel by use of a single parameter, the concentration of the AA in the initial polymer solution. As an added feature, within the concentration of AA investigated, ligand density can be finely tuned without significantly affecting the mechanical properties of the sample.

Taking these results altogether, we selected PEGDA-AA with an AA concentration of 0.3% w/v as the most suitable material to seed intestinal epithelial cells. This selection was based on the material that displayed the maximum number of covalent ligands while attaining the required dimensions for the villi microstructures (at least 400 μm in height)

3.3 Caco-2 cells form a polarized monolayer covering the villi-like microstructures fabricated in PEGDA-AA upon collagen functionalization

PEGDA-AA hydrogel scaffolds were fabricated on glass coverslips and were functionalized with either laminin or collagen, since these are the main components of the epithelial basement membrane. Caco-2 cells were then seeded on top of them. Both laminin and collagen scaffolds allowed cell growth, although only scaffold surfaces functionalized with collagen were consistently covered with a cell monolayer within 48 h of culture. Time-lapse videos recorded 4 h after seeding revealed that most of the cells were initially located at the base of the villi microstructures and they formed a migrating front that climbed up the walls of the villi until the structure was fully covered (Figure 5(a), Supplementary movie M1). After 14 days, cells displayed morphological characteristics of a polarized columnar epithelium along all heights of the villi microstructures, with the presence of F-actin accumulation at the apical-side of the cells (brush border) (Figure 5(b-d)). After 21 days of culture, cells expressed epithelial cell markers such as villin, which characterize microvilli formed in the apical side, zonula occludens-1 (ZO-1), found in tight junctions, and β-catenin, which is found in the basolateral cell membranes, at the proper locations (Figure 6(a)). In flat hydrogels, cells adhered and formed a monolayer within 24 h after seeding. However, after 5 days of culture, cells experienced the partial detaching and the loss of barrier function probably due to the high intercellular forces of Caco-2 cells (Figure S7).

Polarized cells in columnar epithelia are also characterized by elongated cell nuclei, which are oriented perpendicular to the tissue surface.[1] Therefore, cell polarization was also assessed by analysis of nuclei morphology and nuclei orientation with respect to the surface of the microstructures. These data were then compared to data obtained from histological images of villi in human tissue and cells cultured on standard Transwell® membranes. Cell nuclei were significantly more elongated on the cells grown on the 3D scaffolds compared to the cells grown on porous polycarbonate membranes (Figure 6(b)). In addition, cell nuclei were also oriented closer to surface perpendicularity on the 3D scaffolds than on cells cultured on conventional substrates (Figure 6(c)). Overall, cells displayed improved polarization morphology on the 3D scaffolds when compared with standard culturing methodologies based on porous filter membranes in Transwells®. Similar experiments were performed with the MDCK cell line, which also successfully formed a monolayer after 14 d of culture (Figure S8), thus extending the usefulness of PEGDA-AA copolymers to other epithelial cell models.

3.4 Caco-2 cells form a functional tissue barrier on the synthetic PEGDA-AA villi-like microstructures

PEGDA-AA hydrogel scaffolds were fabricated on porous PET membranes and mounted on standard Transwells® (Figure S3). Membranes with pore sizes of 5 μm diameter were used to minimize undesired absorbance and scattering effects interfering with the polymerization process that were observed with membranes of smaller pore size and/or polycarbonate material. When using these membranes and comparing them to samples fabricated on glass coverslips used for characterization purposes, the light intensity through the membrane was reduced by 40%. This attenuation of the UV light intensity significantly affected the microstructure morphology. For the same exposure time, the micropillar height was reduced from 400 to 140 μm (Figure 7(a)). Therefore, the fabrication parameters were optimized to account for the membrane absorption. Due to the light scattering effects produced by the membrane, scaffolds containing micropillars 475 ± 23 μm high joined through a supporting base, were obtained in a single exposure process (Figure 7(b)).

TEER measurements provide information about the integrity of the monolayer of polarized cells and were recorded as a function of the cell culture time. TEER values steadily increased with culture time for both the cells seeded on the 3D scaffolds and the standard monolayers cultured on porous filter membranes (Figure 7(c-d)). This behavior is attributed to the proper formation of a monolayer that is functional as a tissue barrier. TEER values for the cells cultured on the 3D scaffolds were significantly lower than those for the Transwell® control for all of the time points tested. In particular, at 21 days of culture, TEER values of 3D scaffolds were reduced by 10-fold with respect to flat monolayers on porous filter membranes, suggesting that the tight junctions are affected by the 3D topography and on the 3D scaffolds their behaviour approaches *in vivo* values of the human small intestine, reported in the range of 12 to 69 Ω cm^2 [48] (Figure 7(d)). The permeability of the paracellular model compound FD4 was significantly higher in the 3D scaffolds (Figure 7(e)). The PEGDA hydrogel did not influence the

Papp measurements (Figure S9). PEG-based hydrogel scaffolds are characterized by a high porosity and hydrophilicity. Specifically, hydrogels fabricated with 5% (w/v) PEGDA 6 kDa have an average mesh size of 14 nm [49], therefore the scaffold does not represent a barrier to diffusion of molecules such as FD4, with an average diameter of 2.8 nm.

These results are consistent with previous 3D models of the intestinal epithelium [38,50,51], where cells grown on 3D surfaces showed increased leakiness and had TEER values closer to those found *in vivo*.

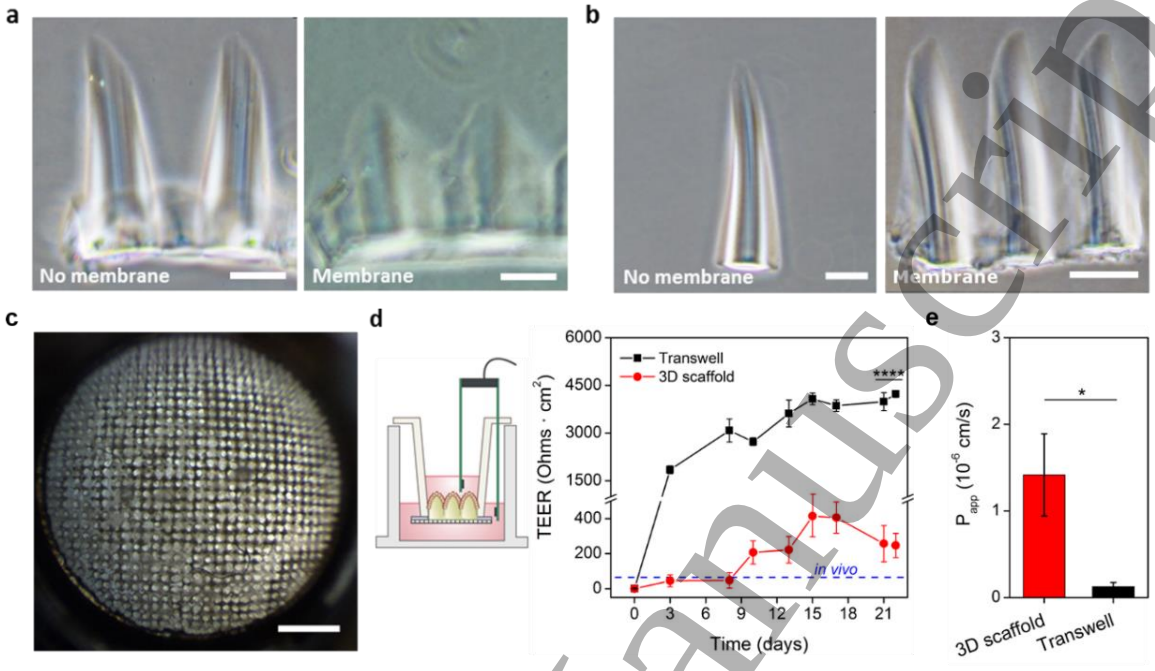

Figure 7. Assembly of 3D scaffolds on modified Transwell® inserts. (a, b) Effect of PET membrane absorption on microstructure morphology compared to glass coverslips used for characterization purposes. PEGDA-AA hydrogels were exposed (a) 120 s for the pillars (plus 15 s of flood exposure to hold pillars together), or (b) 205 s in a single exposure, with or without PET membrane. With the PET membranes, self-standing and joined pillars were obtained in a single fabrication step. (c) Top view of the Caco-2 cell culture on the PEGDA-AA villi-like 3D scaffold assembled on a modified Transwell® insert. (d, e) TEER measurements and permeability of FITC-dextran 4 kDa in epithelial monolayers grown on conventional Transwell® (black) or in PEGDA-AA villi-like 3D scaffolds (red). Mean ± SD, n = 4. Scale bars: a and b = 100 µm; c = 1 mm.

4. Discussion

Tissue equivalents providing cells with a more physiologically relevant microenvironment are in demand for both clinical and *in vitro* testing applications. It is widely recognized that including cell-to-cell and cell-to-matrix interactions, together with proper chemical and mechanical signaling, would benefit the functionality of such constructs [4,5]. However, the complex 3D architectures found in tissues are neglected in most engineered tissues. One of the main reasons limiting the use of 3D tissue microtopography when studying epithelial tissues is the difficulty in producing 3D objects of complex shapes made of soft materials. Conventional microfabrication techniques are ill suited to deliver structures with high aspect ratios and curvature, such as those forming natural epithelial tissues. Methods such as replica molding, 3D printing and photopolymerization have been used to produce scaffolds with 3D topographies for biomedical applications [52,53]. To obtain roundish geometries by replica molding requires complex fabrication design, while avoiding problems demolding soft hydrogels involves the use of intermediate molds and multiple fabrication steps [10]. 3D printing methods are ideal candidates to fabricate complex shapes but are limited in resolution, and require the use of sacrificial materials for manufacturing soft structures [54,55]. Photopolymerization can be used to produce 3D shapes in soft materials by methods such stereolithography or two-photon lithography, but it requires the use of expensive instrumentation [12,53]. Photolithography using 2D photomasks is a low-cost, single-step and parallel fabrication technique that is standardized in the microelectronics field. When applied to materials that undergo radical polymerization, complex shapes can be fabricated by controlling the dynamics of the polymerization reaction through oxygen gradients [16,17]. In this study, we explored this concept further and applied it to a biomedical

set-up. Through this process we obtained, in a single and moldless fabrication procedure, hydrogel microstructures with high aspect ratio (1:6), roundish tip contours, and the anatomical dimensions of small intestine villi. The simplicity and low-cost of the fabrication technique, which only requires a UV lamp and inexpensive acetate photomasks, makes it easily compatible with well-established cell culture systems such as Transwell® inserts. Furthermore, this fabrication process can be easily parallelized, obtaining multiple scaffolds in one single exposure.

PEG-based hydrogels have been extensively investigated as synthetic scaffolds in tissue engineering applications [23]. PEG acrylates photocrosslink in aqueous solutions, forming hydrogels. PEG-derived hydrogels do not withstand protein adsorption, so they are functionalized with peptides or extracellular matrix proteins to allow for cell adhesion and growth. Copolymerization with AA during the crosslinking reaction is an easy method to introduce anchoring groups for cell-adhesive biomolecules. Control of PEG and AA content on properties such as swelling, hydrophilicity and pH sensitivity can be precisely adjusted [20,21]. We observed that the amount of AA had a strong impact on the photopolymerization reaction and can be used as a parameter to modify the polymer growth regime and, ultimately, the shape and dimensions of the microstructures. We have also determined that, within the range of AA concentrations tested, the density of protein ligands incorporated into the hydrogel can be controlled by the AA concentration while leaving the mechanical properties of the structure unaltered. This provides an ideal platform to decouple the influence of mechanical and chemical cues on cell behavior.

In vitro models of the human small intestinal epithelium are routinely used to determine the absorption and metabolism of drugs and these models play a crucial role in preclinical drug development. Conventional systems are based on 2D Caco-2 cell monolayers grown on permeable membranes, and these systems are accepted as standard by pharmaceutical companies and regulatory authorities. However, they lack physiological resemblance and this could lead to incorrect predictions about drug permeability [56]. Numerous attempts, using a variety of materials, have been made to diminish the gap between the conventional 2D models and human intestinal epithelium. Porous poly(lactic-*co*-glycolic) acid (PLGA) scaffolds have been micromolded into villus geometries with high aspect ratios [51,57]. These scaffolds promote epithelial differentiation and absorption [58] but PLGA has mechanical properties outside of the physiological range (E ~ 1-2 GPa). On the other hand, soft collagen hydrogels can be fabricated using a combination of laser ablation and sacrificial molding technique [10,38,50] or by micromolding using PDMS moulds [11]. However, these collagen scaffolds are degraded before the cell culture period needed for complete cell differentiation (usually 21 days for Caco-2 cells). In addition, collagen scaffolds are unsuitable for testing the permeability of rapidly absorbed hydrophobic drugs [38]. The use of synthetic PEG-based hydrogels overcomes limitations on cell culture time, so long-term cell culture experiments are feasible. In addition, photocrosslinkable PEGDA-AA hydrogels offer great versatility to match the cellular requirements of different epithelial tissues. PEGDA chain size and concentration can be used to tune the mechanical properties of the hydrogel within a wide range (E ~ Pa – MPa) [9]. On top of this, the dynamic reaction-diffusion process during the fabrication procedure yields a material with a surface much softer than the bulk. As it has been reported that cells only sense up to 10-20 µm deep [45], this feature can be exploited to produce materials presenting soft 3D environments to the cells while still being mechanically robust and easy to manipulate. The carboxylic groups of acrylic acid can be used to anchor other extracellular matrix proteins such as laminin, which is also a major component of the basement membrane of epithelia. Indeed, we demonstrated that MDCK cells can form a polarized monolayer when grown on laminin functionalized scaffolds. Therefore, PEGDA-AA copolymerized hydrogels appear to be excellent basement membrane surrogates for engineered epithelial tissues. carboxylic groups of acrylic acid can be used to anchor other extracellular matrix proteins such as laminin, which is also a major component of the basement membrane of epithelia. Indeed, we demonstrated that MDCK cells can form a polarized monolayer when grown on laminin functionalized scaffolds. Therefore, PEGDA-AA copolymerized hydrogels appear to be excellent basement membrane surrogates for engineered epithelial tissues.

One of the major limitations of the standard Caco-2 cell model is its high level of resistance, with TEER values up to 1000 Ω cm^2 [59,60], compared to values reported for human intestine (12 to 69 Ω cm^2) [48]. Aberrantly increased TEER values in current *in vitro* models have been attributed to the colon origin of the Caco-2 cell line. While tight junctions of the human small intestine have average pore radius of 6-13 Å, Caco-2 cells display average porosities of only 5 Å [61–63]. However, our results, and those of other researchers, demonstrate that Caco-2 cell monolayers can improve their TEER barrier properties by adding the native tissue architecture [38]. This can modulate the tight barrier properties associated with the curvature of the structures. Theoretical models of epithelial folds are based on evaluation of intraepithelial stresses. These take into account tensions generated at cell-lumen, cell-cell and cell-basement membrane contacts and predict pronounced modulations in cell thickness and cell shape depending on their position along groove-to-crest structure axis [64]. However, *in vivo* leakiness of the tight junctions increases from the tip of the villi to the crypt regions in normal juvenile intestines [65]. Therefore, by including the 3D intestinal architecture, the functional barrier

characteristics of standard cell lines can better mimic those found *in vivo* [38].

5. Conclusion

A photolithography-based process based on dynamic polymerization to fabricate 3D hydrogel microstructures of high-aspect ratio and roundish geometries resembling the villi structures of the small intestinal epithelium is described. Using a polymerization process that controls the timescales of oxygen diffusion and depletion along the irradiation pathway, we demonstrated the production of 3D complex microstructures in a moldless and single fabrication step. The dimensions of the microstructures can be easily adjusted by modifying fabrication parameters such as the polymer composition and irradiation time. In addition, by employing poly(ethylene) glycol diacrylate and acrylic acid copolymers, the ligand density of hydrogel microstructures can be tuned in a simple way without significantly affecting their mechanical properties. The resulting hydrogel microstructures effectively support the growth of epithelial cells until a mature and confluent monolayer is formed. The simple fabrication procedure facilitates its integration with standard characterization techniques. Microstructured hydrogel scaffolds were successfully integrated in a Transwell® system to assess the barrier properties of the biomimetic intestinal epithelium formed. The microfabrication technology described here shows great potential as a method to routinely incorporate 3D structures mimicking microtopographies at the tissue level in cell culture systems.

Acknowledgements

Funding for this project was provided by European Union's Horizon 2020 ERC grant agreement No 647863 (COMIET), the CERCA Programme/ Generalitat de Catalunya (2017-SGR-1079), and the Spanish Ministry of Economy and Competitiveness (TEC2014-51940-C2-2-R, TEC2017-83716-C2-1-R and the Severo Ochoa Program for Centers of Excellence in R&D 2016-2019). M. G.-D. thanks the BEST Postdoctoral Programme, funded by the European Commission under Horizon 2020's Marie Skłodowska-Curie Actions COFUND scheme (Grant Agreement no. 712754) and by the Severo Ochoa programme of the Spanish Ministry of Science and Competitiveness (Grant SEV-2014-0425 (2015-2019)). The collaboration of the MicroFabSpace from IBEC is gratefully acknowledged. Authors thank Raquel Martin-Venegas and Rut Ferrer from the Departament de Bioquímica i Fisiologia, Facultat de Farmàcia i Ciències de l'Alimentació, Universitat de Barcelona (UB) for providing the Caco-2 cells. The results presented here reflect only the views of the authors; the European Commission is not responsible for any use that may be made of the information it contains.

References

[1] Tortora G J and Derrickson B H 2014 *Principles of Anatomy and Physiology* (Wiley Global Education)

[2] Marsh M N and Swift J A 1969 A study of the small intestinal mucosa using the scanning electron microscope *Gut* **10** 940–9

[3] Kelly P, Menzies I, Crane R, Zulu I, Nickols C, Feakins R, Mwansa J, Mudenda V, Katubulushi M, Greenwald S and Farthing M 2004 Responses of small intestinal architecture and function over time to environmental factors in a tropical population. *Am. J. Trop. Med. Hyg.* **70** 412–9

[4] Abbott A 2003 Cell culture: Biology's new dimension *Nature* **424** 870–2

[5] Cushing M C and Anseth K S 2007 Hydrogel cell cultures *Science (80-.).* **316** 1133–4

[6] Justice B A, Badr N A and Felder R A 2009 3D cell culture opens new dimensions in cell-based assays *Drug Discov. Today* **14** 102–7

[7] Elliott N T and Yuan F 2011 A review of three-dimensional in vitro tissue models for drug discovery and transport studies *J. Pharm. Sci.* **100** 59–74

[8] Yu J, Carrier R L, March J C and Griffith L G 2014 Three dimensional human small intestine models for ADME-Tox studies *Drug Discov. Today* **19** 1587–94

[9] Huang G, Wang L, Wang S, Han Y, Wu J, Zhang Q, Xu F and Lu T J 2012 Engineering three-dimensional cell mechanical microenvironment with hydrogels *Biofabrication* **4** 042001

[10] Sung J H, Yu J, Luo D, Shuler M L and March J C 2011 Microscale 3-D hydrogel scaffold for biomimetic gastrointestinal (GI) tract model *Lab Chip* **11** 389–92

[11] Wang Y, Gunasekara D B, Reed M I, DiSalvo M, Bultman S J, Sims C E, Magness S T and Allbritton N L 2017 A microengineered collagen scaffold for generating a polarized crypt-villus architecture of human small intestinal epithelium *Biomaterials* **128** 44–55

[12] Raman R and Bashir R 2015 *Stereolithographic 3D bioprinting for biomedical applications* (Elsevier Inc.)

[13] Chandra D and Crosby A J 2011 Self-wrinkling of UV-cured polymer films *Adv. Mater.* **23** 3441–5

[14] Guvendiren M, Yang S and Burdick J A 2009 Swelling-Induced surface patterns in hydrogels with gradient crosslinking density *Adv. Funct. Mater.* **19** 3038–45

[15] Krutkramelis K, Xia B and Oakey J 2016 Monodisperse polyethylene glycol diacrylate hydrogel microsphere formation by oxygen-controlled photopolymerization in a microfluidic device *Lab Chip* **16** 1457–65

[16] Shim T S, Yang S-M and Kim S-H 2015 Dynamic designing of microstructures by chemical gradient-mediated growth *Nat. Commun.* **6** 6584

[17] Kim J H, Je K, Shim T S and Kim S H 2017 Reaction-Diffusion-Mediated Photolithography for Designing Pseudo-3D Microstructures *Small* **13** 1–11

[18] Viswanathan P, Guvendiren M, Chua W, Telerman S B, Liakath-Ali K, Burdick J A and Watt F M 2016 Mimicking the topography of the epidermal–dermal interface with elastomer substrates *Integr. Biol.* **8** 21–9

[19] Kloxin A M, Kloxin C J, Bowman C N and Anseth K S 2010 Mechanical properties of cellularly responsive hydrogels and their experimental determination *Adv. Mater.* **22** 3484–94

[20] Scott R A and Peppas N A 1999 Compositional effects on network structure of highly cross-linked copolymers of PEG-containing multiacrylates with acrylic acid *Macromolecules* **32** 6139–48

[21] Scott R A and Peppas N A 1999 Kinetics of copolymerization of PEG-containing multiacrylates with acrylic acid *Macromolecules* **32** 6149–58

[22] Li R J and Schork F J 2006 Modeling of the inhibition mechanism of acrylic acid polymerization *Ind. Eng. Chem. Res.* **45** 3001–8

[23] Zhu J 2010 Bioactive modification of poly(ethylene glycol) hydrogels for tissue engineering *Biomaterials* **31** 4639–56

[24] Xu K, Fu Y, Chung W, Zheng X, Cui Y, Hsu I C and John W 2012 Thiol – ene-based biological / synthetic hybrid biomatrix for 3-D living cell culture *Acta Biomater.* **8** 2504–16

[25] Pierce B F, Tronci G, Rößle M, Neffe A T, Jung F and Lendlein A 2012 Photocrosslinked Co-Networks from Glycidylmethacrylated Gelatin and Poly(ethylene glycol) Methacrylates *Macromol. Biosci.* **12** 484–93

[26] Fonseca K B, Gomes D B, Lee K, Santos S G, Sousa A, Silva E A, Mooney D J, Granja P L and Barrias C C 2014 Injectable MMP-Sensitive Alginate Hydrogels as hMSC Delivery Systems *Biomacromolecules* **15** 380–90

[27] Anon http://medcell.med.yale.edu/systems_cell_biology/gi_tract_lab.php

[28] Schneider C A, Rasband W S and Eliceiri K W 2012 NIH Image to ImageJ: 25 years of image analysis *Nat. Methods* **9** 671–5

[29] Decker C and Jenkins A D 1985 Kinetic Approach of O2 Inhibition in Ultraviolet and Laser Induced Polymerizations *Macromolecules* 1241–4

[30] Ligon S C, Husar B, Wutzel H, Holman R and Liska R 2014 Strategies to Reduce Oxygen Inhibition in Photoinduced Polymerization *Chem. Rev.* **114** 557–89

[31] Liu M, Li M De, Xue J and Phillips D L 2014 Time-resolved spectroscopic and density functional theory study of the photochemistry of Irgacure-2959 in an aqueous solution *J. Phys. Chem. A* **118** 8701–7

[32] Lim K S, Schon B S, Mekhileri N V., Brown G C J, Chia C M, Prabakar S, Hooper G J and Woodfield T B F 2016 New Visible-Light Photoinitiating System for Improved Print Fidelity in Gelatin-Based Bioinks *ACS Biomater. Sci. Eng.* **2** 1752–62

[33] O'Brien L E, Zegers M M P and Mostov K E 2002 Building epithelial architecture: Insights from three-dimensional culture models *Nat. Rev. Mol. Cell Biol.* **3** 531–7

[34] Klein G, Langegger M, Timpl R and Ekblom P 1988 Role of laminin a chain in the development of epithelial cell polarity *Cell* **55** 331–41

[35] Schuger L, Yurchenco P, Relan N K and Yang Y 1998 Laminin fragment E4 inhibition studies: Basement membrane assembly and embryonic lung epithelial cell polarization requires laminin polymerization *Int. J. Dev. Biol.* **42** 217–20

[36] Weaver V M, Petersen O W, Wang F, Larabell C A, Briand P, Damsky C and Bissell M J 1997 Reversion of the malignant phenotype of human breast cells in three-dimensional culture and in vivo by integrin blocking antibodies *J. Cell Biol.* **137** 231–45

[37] Hidalgo I J, Raub T J and Borchardt R T 1989 Characterization of the human colon carcinoma cell line (Caco-2) as a model system for intestinal epithelial permeability *Gastroenterology* **96** 736–49

[38] Yu J, Peng S, Luo D and March J C 2012 In vitro 3D human small intestinal villous model for drug permeability determination *Biotechnol. Bioeng.* **109** 2173–8

[39] Sung J H, Yu J, Luo D, Shuler M L and March J C 2011 Microscale 3-D hydrogel scaffold for biomimetic gastrointestinal (GI) tract model *Lab Chip* **11** 389–92

[40] Madaghiele M, Marotta F, Demitri C, Montagna F, Maffezzoli A and Sannino A 2014 Development of semi- and grafted interpenetrating polymer networks based on poly(ethylene glycol) diacrylate and collagen *J. Appl. Biomater. Funct. Mater.* **12** 183–92

[41] Park S, Lee H J and Koh W-G G 2012 Multiplex Immunoassay Platforms Based on Shape-Coded Poly(ethylene glycol) Hydrogel Microparticles Incorporating Acrylic Acid *Sensors (Switzerland)* **12** 8426–36

[42] Wu Y, Liang J, Horkay F and Libera M 2016 Antimicrobial loading into and release from poly(ethylene glycol)/poly(acrylic acid) semi-interpenetrating hydrogels *J. Polym. Sci. Part B Polym. Phys.* **54** 64–72

[43] Liao D, Yang J, Zhao J, Zeng Y, Vinter-Jensen L and Gregersen H 2003 The effect of epidermal growth factor on the incremental Young's moduli in the rat small intestine *Med. Eng. Phys.* **25** 413–8

[44] Browe D P, Wood C, Sze M T, White K A, Scott T, Olabisi R M and Freeman J W 2017 Characterization and optimization of actuating poly(ethylene glycol) diacrylate/acrylic acid hydrogels as artificial muscles *Polym. (United Kingdom)* **117** 331–41

[45] Kuo C H R, Xian J, Brenton J D, Franze K and Sivaniah E 2012 Complex stiffness gradient substrates for studying mechanotactic cell migration *Adv. Mater.* **24** 6059–64

[46] Wang W H, Dong J L, Baker G L and Bruening M L 2011 Bifunctional polymer brushes for low-bias enrichment of mono- and multi-phosphorylated peptides prior to mass spectrometry analysis *Analyst* **136** 3595–8

[47] De Campos Vidal B and Mello M L S 2011 Collagen type I amide I band infrared spectroscopy *Micron* **42** 283–9

[48] Ferrec E, Chesne C, Artusson P, Brayden D, Fabre G, Gires P, Guillou F and Rousset M 2001 In Vitro Models of the Intestinal Barrier *Atla* **29** 649–68

[49] Durst C A, Cuchiara M P, Mansfield E G, West J L and Grande-Allen K J 2011 Flexural characterization of cell encapsulated PEGDA hydrogels with applications for tissue engineered heart valves *Acta Biomater.* **7** 2467–76

[50] Kim S H, Chi M, Yi B, Kim S H, Oh S, Kim Y, Park S and Sung J H 2014 Three-dimensional intestinal villi epithelium enhances protection of human intestinal cells from bacterial infection by inducing mucin expression. *Integr. Biol. (Camb).* **6** 1122–31

[51] Costello C M, Hongpeng J, Shaffiey S, Yu J, Jain N K, Hackam D and March J C 2014 Synthetic small intestinal scaffolds for improved studies of intestinal differentiation *Biotechnol. Bioeng.* **111** 1222–32

[52] Yanagawa F, Sugiura S and Kanamori T 2016 Hydrogel microfabrication technology toward three dimensional tissue engineering *Regen. Ther.* **3** 45–57

[53] Zorlutuna P, Annabi N, Camci-Unal G, Nikkhah M, Cha J M, Nichol J W, Manbachi A, Bae H, Chen S and Khademhosseini A 2012 Microfabricated biomaterials for engineering 3D tissues *Adv. Mater.* **24** 1782–804

[54] Murphy S V. and Atala A 2014 3D bioprinting of tissues and organs *Nat. Biotechnol.* **32** 773–85

[55] O'Bryan C S, Bhattacharjee T, Niemi S R, Balachandar S, Baldwin N, Ellison S T, Taylor C R, Sawyer W G and

Angelini T E 2017 Three-dimensional printing with sacrificial materials for soft matter manufacturing *MRS Bull.* **42** 571–7

[56] Artursson P, Palm K and Luthman K 2001 Caco-2 monolayers in experimental and theoretical drug transport predictions of drug transport *Adv. Drug Deliv. Rev.* **46** 27–43

[57] Costello C M, Sorna R M, Goh Y, Cengic I, Jain N K and March J C 2015 3-D Intestinal Scaffolds for Evaluating the Therapeutic Potential of Probiotics *Mol. Pharm.* **11** 2030–9

[58] Shaffiey S A, Jia H, Keane T, Costello C, Wasserman D, Quidgley M, Dziki J, Badylak S, Sodhi C P, March J C and Hackam D J 2016 Intestinal stem cell growth and differentiation on a tubular scaffoldwith evaluation in small and large animals *Regen. Med.* **11** 45–61

[59] Sun H, Chow E C, Liu S, Du Y and Pang K S 2008 The Caco-2 cell monolayer: usefulness and limitations. *Expert Opin. Drug Metab. Toxicol.* **4** 395–411

[60] Boegh M, Foged C, Müllertz A and Mørck Nielsen H 2013 Mucosal drug delivery: barriers, in vitro models and formulation strategies *J. Drug Deliv. Sci. Technol.* **23** 383–91

[61] Calatayud M, Vázquez M, Devesa V and Vélez D 2012 In vitro study of intestinal transport of inorganic and methylated arsenic species by Caco-2/HT29-MTX cocultures *Chem. Res. Toxicol.* **25** 2654–62

[62] Han L, Zhao Y, Yin L, Li R, Liang Y, Huang H, Pan S, Wu C and Feng M 2012 Insulin-Loaded pH-Sensitive Hyaluronic Acid Nanoparticles Enhance Transcellular Delivery *AAPS PharmSciTech* **13** 836–45

[63] Tavelin S, Taipalensuu J, Söderberg L, Morrison R, Chong S and Artursson P 2003 Prediction of the oral absorption of low-permeability drugs using small intestine-like 2/4/A1 cell monolayers *Pharm. Res.* **20** 397–405

[64] Štorgel N, Krajnc M, Mrak P, Štrus J and Ziherl P 2016 Quantitative Morphology of Epithelial Folds *Biophys. J.* **110** 269–77

[65] Schulzke J-D, Bentzel C J, Schulzke I, Riecken E-O and Fromm M 1998 Epithelial Tight Junction Structure in the Jejunum of Children with Acute and Treated Celiac Sprue *Pediatr. Res.* **43** 435–41